INSTITUTE OF PHYSICS PUBLISHING PHYSICS IN MEDICINE AND BIOLOGY

Phys. Med. Biol. **50** (2005) 3787–3806 doi:10.1088/0031-9155/50/16/009

A finite difference method with reciprocity used to incorporate anisotropy in electroencephalogram dipole source localization

Hans Hallez[1,3], Bart Vanrumste[2], Peter Van Hese[1,3], Yves D'Asseler[1], Ignace Lemahieu[1] and Rik Van de Walle[1]

[1] Department of Electronics and Information Systems, Medical Image and Signal Processing (MEDISIP) Ghent University, Sint-Pietersnieuwstraat 41, 9000 Ghent, Belgium
[2] Department of Electrical Engineering, KU Leuven, Kasteelpark Arenberg 10, 3001 Leuven, Belgium
[3] Department of Neurology, Ghent University Hospital, De Pintelaan 135, 9000 Ghent, Belgium

Received 1 April 2005, in final form 9 June 2005
Published 28 July 2005
Online at stacks.iop.org/PMB/50/3787

Abstract

Many implementations of electroencephalogram (EEG) dipole source localization neglect the anisotropical conductivities inherent to brain tissues, such as the skull and white matter anisotropy. An examination of dipole localization errors is made in EEG source analysis, due to not incorporating the anisotropic properties of the conductivity of the skull and white matter. First, simulations were performed in a 5 shell spherical head model using the analytical formula. Test dipoles were placed in three orthogonal planes in the spherical head model. Neglecting the skull anisotropy results in a dipole localization error of, on average, 13.73 mm with a maximum of 24.51 mm. For white matter anisotropy these values are 11.21 mm and 26.3 mm, respectively. Next, a finite difference method (FDM), presented by Saleheen and Kwong (1997 *IEEE Trans. Biomed. Eng.* **44** 800–9), is used to incorporate the anisotropy of the skull and white matter. The FDM method has been validated for EEG dipole source localization in head models with all compartments isotropic as well as in a head model with white matter anisotropy. In a head model with skull anisotropy the numerical method could only be validated if the 3D lattice was chosen very fine (grid size $\leqslant$2 mm).

(Some figures in this article are in colour only in the electronic version)

1. Introduction

Electroencephalogram (EEG) dipole source localization has proven to be a valuable tool in the pre-surgical evaluation of patients suffering from epilepsy (Boon *et al* 1996) and event-related potentials or ERPs (Scherg 1992). This technique can make an estimate of the active

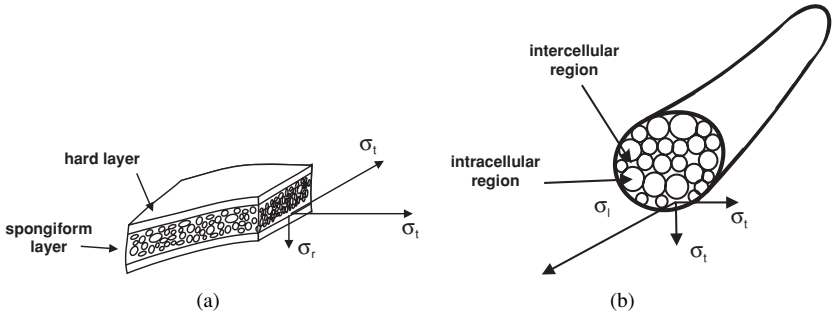

Figure 1. The anisotropic properties of the conductivity of skull and white matter tissues. (a) The skull consists of three layers: a spongiform layer between two hard layers. The conductivity tangentially to the skull surface is 10 times larger than the radial conductivity. (b) White matter consists of axons, grouped in bundles. The conductivity along the nerve bundle is 9 times larger than perpendicular to the nerve bundle.

anatomical zone based on the measured EEG. EEG dipole source localization consists of two subproblems, i.e., the forward and the inverse problem. The forward problem calculates the electrode potentials in a head model, given the source(s) (usually a current dipole).

On the other hand, the inverse problem is solved by finding the dipole which best represents the given potentials at the scalp electrodes. This can be performed by iteratively modifying the dipole parameters, until for a given set of parameters, the associated potentials (found by the forward problem) best represent the measured potentials.

Besides the current dipole, as a model for active neurons, a volume conductor model is required to perform EEG source localization of the human head. The earliest model used was the three-shell spherical head model, consisting of a brain compartment, a skull compartment and a scalp compartment (Salu *et al* 1990). An analytical expression exists to solve the forward problem in those head models. In the last decade more realistic shaped head models have been used (Huiskamp *et al* 1999, Yvert *et al* 1997). These models are based on segmented 3D magnetic resonance images. It has been shown that the dipole localization error between spherical and realistic head models is on average 2 cm (Yvert *et al* 1997). Recently, the ratio of the conductivity value of the skull compartment to the conductivity value of the brain compartment has been updated from 1/80 compared with the brain compartment to 1/16 (Ferree *et al* 2000). Dipole localization differences of 30 mm were reported (Vanrumste *et al* 2000) due to utilizing older values instead of the newer ones.

The conductivity of skull tissue and white matter is direction dependent or anisotropic (see figure 1). Furthermore, it is well known that skull tissue has an anisotropic conductivity with a ratio of up to 1:10 (radially:tangentially to the skull surface) (Wolters *et al* 2001). For white matter, a similar anisotropy ratio is known. Haueisen *et al* and Wolters *et al* showed that white matter anisotropy has an influence on the forward solution for EEG and MEG (Wolters *et al* 2001, Haueisen *et al* 2002). In these studies, the authors concluded that the anisotropic conductivities should not be neglected. Note that there are analytical expressions available that can incorporate tangential and radial conductivity in a multi-shell spherical head model (de Munck and Peters 1993).

Techniques able to solve the forward problem in a realistically shaped head model with anisotropic conducting compartments are the finite difference method (FDM) and the finite element method (FEM). In contrast, the boundary element method (BEM) can only be used if the compartments are assumed isotropic. Our preference goes to FDM as it uses a regular 3D cubic grid, which can easily be extracted from the MR images. Furthermore, FDM requires

no tessellation, which may be troublesome in 3D volumes. Although the FEM results are comparable with FDM results from the same grid, the computational expense of FDM is much smaller than that of FEM (Darvas *et al* 2004). Using the mutual dependence of the input and the output of the forward problem or reciprocity, the number of forward calculations can be significantly reduced. This leads to a substantial reduction of the calculation time compared to the procedure in which for each forward evaluation in the inverse problem, a potential distribution needs to be calculated numerically (Vanrumste *et al* 2001). To our knowledge, this is the first time that FDM with reciprocity has been used to incorporate anisotropic conductivity values in EEG dipole source localization.

The aim of the study is to assess whether FDM with reciprocity (FDM-R) can be used to perform EEG dipole localization in a head model with an anisotropic skull and a white matter compartment. This is carried out by inspecting dipole localization errors which are solely due to the discretization of the spherical head model and discretization of anisotropy values in a five-shell spherical head model.

These errors are compared with those found by not incorporating an anisotropic compartment in a five-shell spherical head model. In this reference model the errors are solely due to not incorporating anisotropy.

2. Incorporating anisotropy into the finite difference method

2.1. The forward problem

Solving the forward problem in EEG dipole source localization results in the electric potentials, caused by the current dipole in a volume conductor, representing the human head. The solution to Poisson's differential equation yields the electric potentials (Sarvas 1987),

$$\nabla \cdot (\sigma(x, y, z) \cdot \nabla V(x, y, z)) = I\delta(\mathbf{r} - \mathbf{r}_1) - I\delta(\mathbf{r} - \mathbf{r}_2), \tag{1}$$

where $V(x, y, z)$ is the potential distribution inside the head model, $\sigma(x, y, z)$ denotes the conductivity tensor which is place dependent, $\delta(t)$ is the Dirac function and $\mathbf{r}_1, \mathbf{r}_2$ are the location coordinates of the current source and current sink of the dipole, respectively. Important to note is that the relationship between the electrode potentials $\mathbf{V}_{\text{dipole}} \in \Re^{m\times 1}$ (m being the number of electrodes), the dipole location, $\mathbf{r} = (x, y, z)^T \in \Re^{3\times 1}$, and the dipole moments, $\mathbf{d} = (d_x, d_y, d_z)^T \in \Re^{3\times 1}$, can always be written as follows, regardless of the specific head model used,

$$\mathbf{V}_{\text{dipole}} = \mathbf{L}(\mathbf{r}) \cdot \mathbf{d}, \tag{2}$$

where $\mathbf{L}(\mathbf{r}) \in \Re^{m\times 3}$ is the lead-field matrix for a dipole at location $\mathbf{r}$.

As mentioned in the introductory part, the forward problem can be solved by an analytical expression, for spherical head models, or by numerical methods, for realistic head models. An analytical expression, which can handle anisotropic conductivities, has been presented by de Munck and Peters (1993). This expression uses a finite sum of Legendre terms. However, the analytical expression can only be used in spherical head models and the anisotropy in the conductivities is limited to a radial and a tangential direction.

2.2. The finite difference method (FDM)

Numerical methods use a computational grid or lattice to solve the forward problem. For FDM the head is tessellated in a cubic grid, where each cube has the same size. Each cubic element has a conductivity tensor allocated, depending on the compartment to which it belongs. In this study, we used four kinds of compartments: scalp, skull, white matter and grey matter. Only

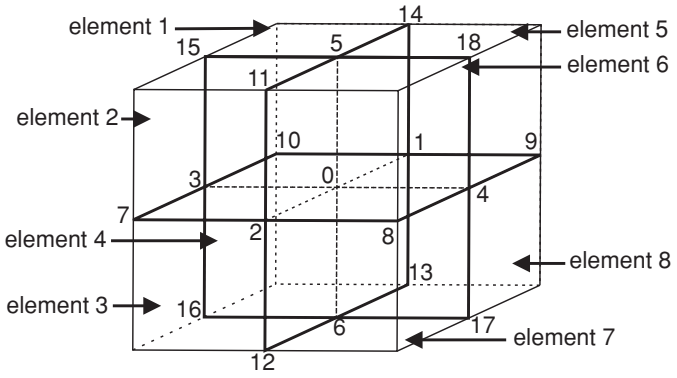

Figure 2. The potential at node 0 can be written as a linear combination of the 18 neighbouring nodes in the FDM scheme.

the scalp and grey matter compartments are considered isotropic throughout the study. For isotropic tissues the conductivity tensor becomes a scalar. However, for anisotropic conducting tissues, the conductivity tensor can vary for different positions in the anisotropic compartment.

In the multi-shell spherical head model the conductivity tensor in the skull and white matter compartment is a diagonal matrix. If we assume that the local coordinate system is in the radial and tangential direction, then the conductivity tensor at an element j can be written as follows

$$\sigma^j_{\text{sph}} = \begin{pmatrix} \sigma_r^j & 0 & 0 \\ 0 & \sigma_t^j & 0 \\ 0 & 0 & \sigma_t^j \end{pmatrix},$$

where σ_t^j and σ_r^j are the conductivities in the tangential and radial direction at element j, respectively. The matrix representation has to be transformed to a global Cartesian coordinate system of the head, equal for all elements. Therefore a rotation matrix has to be applied. The matrix representation of the conductivity tensor at element j in the Cartesian system of the head is then given by $\sigma^j_{\text{head}} = \mathbf{T_j}^T \sigma^j_{\text{sph}} \mathbf{T_j}$, where T is a rotation transfer matrix from the local coordinate system to the global coordinate system (Hinchey 1976).

A finite difference method which can handle these properties has been presented by Saleheen and Kwong (1998). The method differs from the finite difference method, which puts the computational points at the centre of the elements, in that it calculates the potential values at the nodes of the elements.

Basically, the method states that in a 3D cubic lattice, the potential value at point 0 can be written as a linear combination of potential values at 18 neighbours according to figure 2. Thus, Poisson's equation (1) can be approximated in a finite difference calculation scheme as follows,

$$\sum_{i=1}^{18} a_i \phi_i - \left(\sum_{i=1}^{18} a_i \right) \phi_0 = I\delta(\mathbf{r} - \mathbf{r}_1) - I\delta(\mathbf{r} - \mathbf{r}_2), \tag{3}$$

where ϕ_i is the discrete potential value at node i. Note that we use V for continuous potential values and ϕ for discrete potential values. a_i are the coefficients depending on the conductivity tensor of the elements and the internode distance. These coefficients are given in Saleheen and Kwong (1998). The dipole source is characterized by the right-hand side of the equation.

The current injected or removed is denoted by I and the location of the current source and sink is denoted by $\mathbf{r}_1$ and $\mathbf{r}_2$, respectively. The location of node at 0 is denoted by $\mathbf{r}$.

At nodes at the corners of the compartment as illustrated in figure 2 (for example node 11), the boundary normal cannot obviously be defined. Hence, other procedures need to be used to derive the finite difference equations. The study uses the 'transition layer' method to remove singularities in spatial derivatives of the conductivities in order to derive the finite difference approximation of Laplace's equation for the configuration in figure 2. This has an advantage if we want to enforce a Neumann boundary condition in the forward problem: the FDM formulation allows a discrete change or discontinuity in conductivity between neighbouring elements and will automatically incorporate the boundary between two different materials (Saleheen and Kwong 1998).

For each computational point a linear equation can be written as in equation (3), and for all computational points we obtain a set of linear equations which can be written as follows: $\mathbf{A} \cdot \mathbf{V} = \mathbf{I}$. The matrix $\mathbf{A} \in \Re^{n \times n}$ is the stiffness matrix and is dependent on the isotropic or anisotropic conductivities at the elements. The $\mathbf{I} \in \Re^{n \times 1}$ is the array which denotes the current source and sink. The current source and current sink at i and j are indicated by $\mathbf{I}(i) = I$ and $\mathbf{I}(j) = -I$, respectively. All remaining elements are zero. n is the number of computational points. Furthermore, the stiffness matrix A is sparse as for each row there are at most 18 off-diagonal elements non-zero. We wish to solve this system for $V \in \Re^{n \times 1}$.

2.3. Successive overrelaxation

To solve this large sparse linear system, iterative methods need to be used. We have utilized successive overrelaxation (SOR) (Barrett *et al* 1994). The SOR is a method for solving a linear system of equations and is derived from an extrapolation to the Gauss–Seidel method. This extrapolation takes the form of a weighted average between the previous iterate, $\phi_i^{(k-1)}$, and the computed Gauss–Seidel iterate successively for each component,

$$\phi_i^{(k)} = \omega \bar{\phi}_i^{(k)} + (1 - \omega)\phi_i^{(k-1)}, \tag{4}$$

where $\bar{x}$ is the Gauss–Seidel iterate, and ω is the extrapolation factor. After j iterations, the node potentials, $\phi_i^{(j)}$, $\forall 1 \leqslant i \leqslant n$, will be equal to $\Phi_\mathbf{j} = (\phi_\mathbf{0}, \phi_\mathbf{1}, \ldots, \phi_\mathbf{n})$. The iteration is terminated when the residual ($r_j = \|\mathbf{A}\Phi_\mathbf{j} - \mathbf{I}\|$) stops decreasing. An optimal extrapolation factor ω_{opt}, which yields a minimum of iterations to satisfy the termination criterion, is dependent on the grid size. From tests, we have found that the extrapolation factor used in SOR with values $\omega = 1.93, \omega = 1.95$ and $\omega = 1.97$ for a grid size of 3, 2 and 1 mm, respectively, yields in general the smallest number of iterations. An implementation has been made in Matlab and the calculation time for a grid size of 3, 2 and 1 mm takes typically 15 min, 2 h and 6 h respectively (Pentium 4, 2.6 GHz, 2 GBytes RAM).

2.4. Reciprocity

It would be too time-consuming to solve the forward problem for each dipole position and orientation utilizing successive overrelaxation. Therefore, the reciprocity theorem is used to reduce the number of forward calculations. Reciprocity was introduced in EEG source analysis by Rush and Driscoll (1969). Reciprocity describes the relation of mutual dependence of the input and the output of the linear system: the voltage between two electrodes at the surface due to a current source and current sink infinitesimally close to each other (dipole configuration), equals the voltage between these two points due to a unit current at the initial electrodes (Malmivuo and Plonsey 1995). By solving only one forward calculation numerically, by

introducing current monopoles at an electrode pair, and storing the obtained node potentials or lead-field (which is the gradient of the potential field) in a data structure, one can obtain the potential difference at the electrode pair for every dipole position and orientation as follows,

$$U_{AB}(\mathbf{r}, \mathbf{d}) = \frac{\mathbf{d}^T \cdot \nabla V(\mathbf{r})}{I_{AB}}, \tag{5}$$

with U_{AB} the potential difference between the scalp electrodes A and B generated by the dipole at position $\mathbf{r}$ and with moment $\mathbf{d}$. I_{AB} is a fictive unit current which enters at electrode A and leaves at electrode B. When $\mathbf{r}$ does not coincide with a node, then $\nabla V(\mathbf{r})$ is obtained with trilinear interpolation.

If l scalp electrodes are used to measure the EEG, $l - 1$ electrode pairs can be found with linear independent potential differences. Therefore $l - 1$ numerical forward calculations are performed and stored. The $l - 1$ potential differences at the $l - 1$ electrode pairs are then transformed in l average referenced potentials at the l electrodes. Together with the finite difference method (FDM-R) we will use this to perform simulations, described further on.

2.5. The inverse problem

Solving the inverse problem consists in finding the parameters of the dipole source that best explain a set of measured potentials. We find the optimal position $\mathbf{r}_{\text{opt}}$ and moment $\mathbf{d}_{\text{opt}}$ for the input potentials $\mathbf{V}_{\text{in}} \in \mathbb{R}_{k\times 1}$ at k scalp electrodes. This is done by minimizing the relative residual energy (RRE) (Vanrumste *et al* 2000),

$$\text{RRE} = \frac{\|\mathbf{V}_{\text{in}} - \mathbf{V}_{\text{model}}(\mathbf{r}, \mathbf{d})\|}{\|\mathbf{V}_{\text{in}}\|} + C(\mathbf{r}), \tag{6}$$

where $\mathbf{V}_{\text{model}} \in \mathbb{R}^{k\times 1}$ are the average referenced potentials obtained from the forward model. $\|\cdot\|$ indicates the L_2-norm. $C(\mathbf{r})$ is zero for dipole positions in the brain compartment (the cortical shell, white matter shell and thalamic shell) and is set to a high value elsewhere. This additional term will restrict the solution of the inverse solver to the brain compartment. The Nelder–Mead simplex method is used to find the global minimum of the RRE, because of its simplicity and robustness against local minima (Press *et al* 1995) .

3. Methods

In our study we used a five-shell spherical head model, with the following compartments: the thalamic inner sphere, white matter sphere, cortical sphere, skull and the scalp, with radii of 20, 70, 80, 86 and 92 mm respectively. Only the white matter sphere and the skull were made anisotropic. Figure 3 illustrates the five-shell spherical head model. The electrodes were placed according to the standard 10–20 system with six additional electrodes on the temporal region.

For the FDM-R method we divided the five-shell spherical head model into cubic grids of 3, 2 and 1 mm. By using a fine grid we can assume that the dipole localization errors due to electrode mislocation are negligible, hence there will always be a lattice point at an electrode location. Test dipoles were placed in the grey matter inner sphere, white matter sphere and grey matter outer sphere, distributed along the axial (*XY*), sagittal (*YZ*) and coronal (*XZ*) plane. The *X*-, *Y*- and *Z*-axis are oriented along the left–right, back–front and bottom–top direction of the head model, respectively. The distance between the test dipoles was 5 mm. In the *XY* plane there were 777 test dipoles and in the *XZ* and *YZ* plane there were 586 dipoles. We did not consider test dipoles that were inferior than the most inferior electrode position.

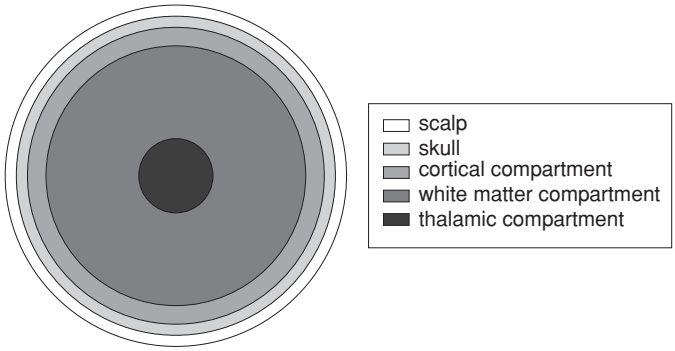

Figure 3. The five-shell spherical head model. The different compartments are indicated by the different greyscale values. In the present study, the skull and the white matter compartment can be set to isotropic or anisotropic conductivites. The other compartments are all set to the isotropic conductivity.

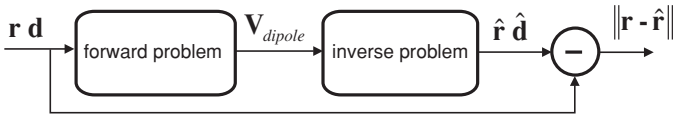

Figure 4. A flowchart of the simulation study where the dipole localization error is investigated due to the differences between the head models used in the forward problem and in the inverse problem. Also the solution can be obtained by an analytical formula or by the numerical method, FDM-R.

For each location, we also considered three orientations according to the Cartesian coordinate system: the X-, Y-, Z-orientation. The total number of test dipoles is $(777+2\times586)\times3 = 5847$, for each head model.

The radial σ_r and tangential conductivities σ_t are calculated using the volume constraint, which is explained in the appendix. The volume constraint states that the volume of the anisotropic conductivity ellipsoid should be equal to the volume of the isotropic conductivity sphere. For the isotropic conductivity values we use $\sigma^{\text{brain}}_{\text{isotropic}} = 0.33$ S m^{-1} for the brain compartment, $\sigma^{\text{skull}}_{\text{isotropic}} = \sigma^{\text{brain}}_{\text{isotropic}}/16 = 0.020$ S m^{-1} for the skull compartment and $\sigma^{\text{scalp}}_{\text{isotropic}} = 0.33$ S m^{-1} for the scalp (Gonçalves *et al* 2003, Ferree *et al* 2000). For the skull we use a radial conductivity of $\sigma^{\text{skull}}_r = 0.004\,309$ S m^{-1} and a tangential conductivity of $\sigma^{\text{skull}}_t = 10\sigma^{\text{skull}}_r = 0.043\,09$ S m^{-1}. In the white matter compartment we modelled the white matter anisotropy as nerve fibres that originate at the edge of the inner grey matter compartment and go radial to the edge of the outer grey matter compartment. Here we use a radial conductivity of $\sigma^{\text{brain}}_r = 1.4278$ S m^{-1} and a tangential conductivity of $\sigma^{\text{brain}}_t = 0.15864$ S m^{-1}.

3.1. Dipole localization errors due to omitting an anisotropic conductivity

First we investigated dipole localization errors due to incorporating an isotropic instead of an anisotropic conducting compartment. The dipole localization errors of this part of the study are used as a reference for the following simulations. The setup of this simulation study can be made from a general setup, shown in figure 4. The potentials at the electrodes were calculated

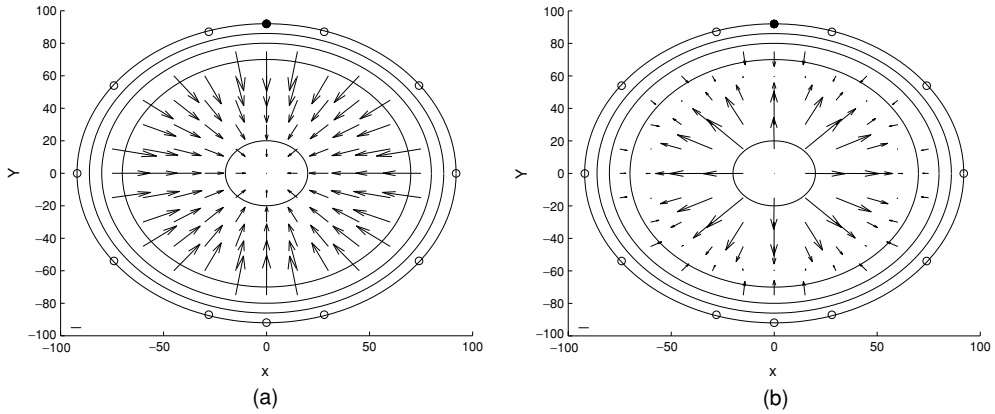

Figure 5. (a) The dipole localization error due to using an isotropic skull conductivity instead of an anisotropic one. (b) The dipole localization error due to using an isotropic white matter conductivity instead of an anisotropic one. The localization error in both figures is represented as an arrow in each test dipole: the tail of the arrow shows the original position while the tip shows the fitted position; the plane of dipoles was in the *XY* plane and the orientation of the test dipole was oriented along the *X*-axis. For other planes of dipoles and other dipole orientations, we obtain similar results.

by using the analytical expression for a given dipole in the brain compartments in a five-shell spherical head model with skull or white matter compartment being anisotropic. Next, for the set of potential values at the 27 electrodes, the dipole parameters were estimated for a five-shell spherical head model but with the initial anisotropic conducting compartment set to isotropic. The dipole localization errors were then inspected.

3.2. Dipole localization errors due to using FDM-R in a spherical head model with isotropic conducting compartments

The aforementioned numerical method was validated in isotropic conducting compartments. We applied the analytical expression for a given dipole in the brain compartments in a five-shell spherical head model with all compartments set to isotropic. The resulting electrode potentials were then used to solve the inverse problem in a five-shell spherical head model with all compartments set to isotropic, but using FDM-R. The simulation set-up can be obtained by using an analytic formula in the forward problem and the FDM-R method for the inverse problem in figure 4. Here also, the dipole localization errors were then inspected.

3.3. Dipole localization errors due to using FDM-R in a five-shell spherical head model with anisotropic conducting compartments

Finally, we validated the aforementioned numerical method, FDM-R, in the five-shell spherical head model with skull or white matter compartments set to anisotropic conductivity values. The flowchart of this simulation study can be derived from figure 4: the potentials at the electrodes were calculated by using the analytical expression for a given dipole in the brain compartments in a five-shell spherical head model with skull or white matter compartments set to anisotropic conducting values and all other compartments set to isotropic. Next, using FDM-R the inverse problem was solved for the set of potentials in a five-shell spherical head

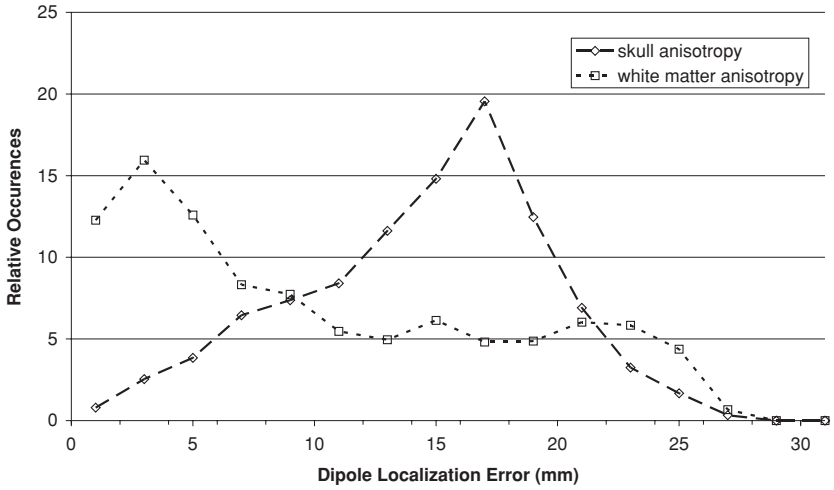

Figure 6. The histogram of the dipole localization error for not including skull and white matter anisotropy. On the horizontal axis the dipole localization error is denoted in mm. The bins are 2 mm wide. The *y*-axis indicates the percentage of dipoles which belongs to a range of dipole localization errors indicated by the bin.

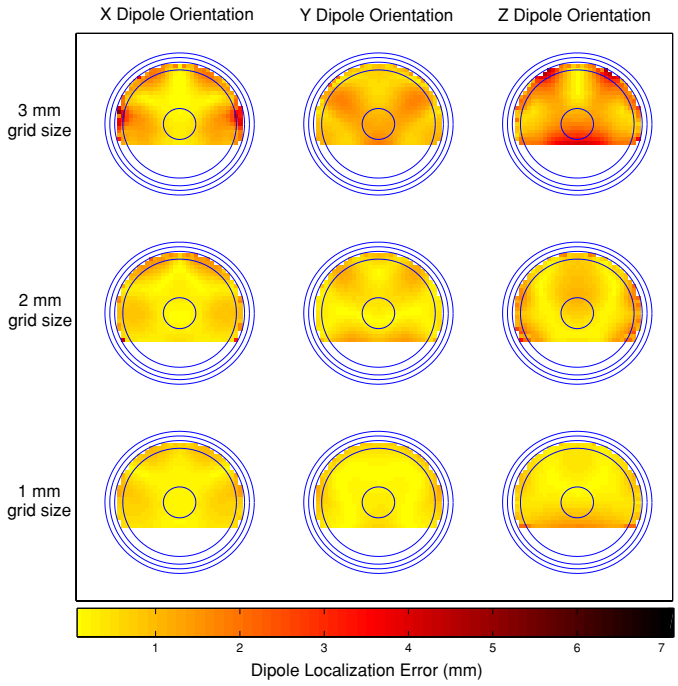

Figure 7. The dipole localization error mapped on the *XZ* planes for FDM-R in an isotropic spherical head model. The first, second and third columns are the dipole localization errors of all dipoles oriented along the *X*-axis, *Y*-axis and *Z*-axis, respectively. The upper, middle and bottom rows represent grid sizes of 3 mm, 2 mm and 1 mm, respectively.

model with the initial anisotropic compartment set to anisotropic conducting values. The dipole localization errors were then inspected.

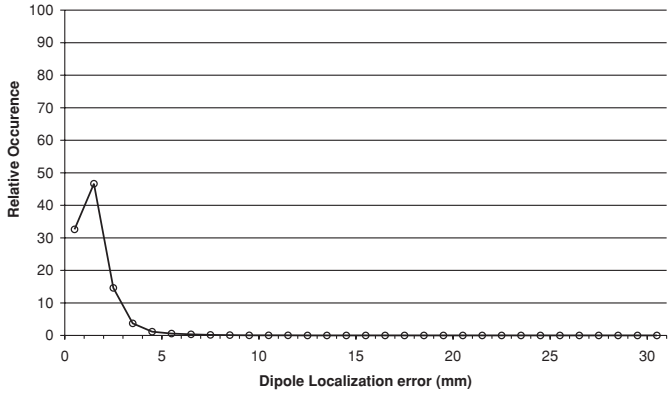

(a)

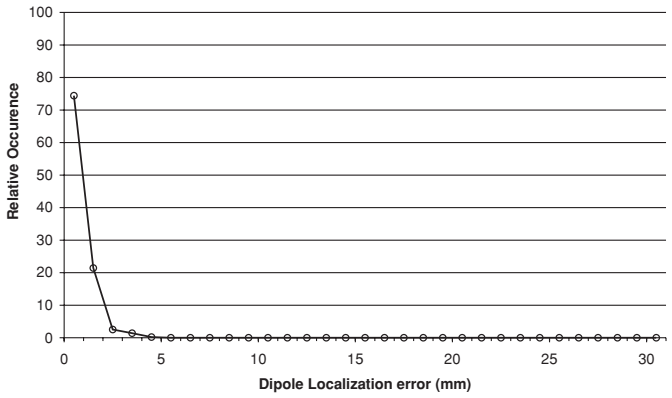

(b)

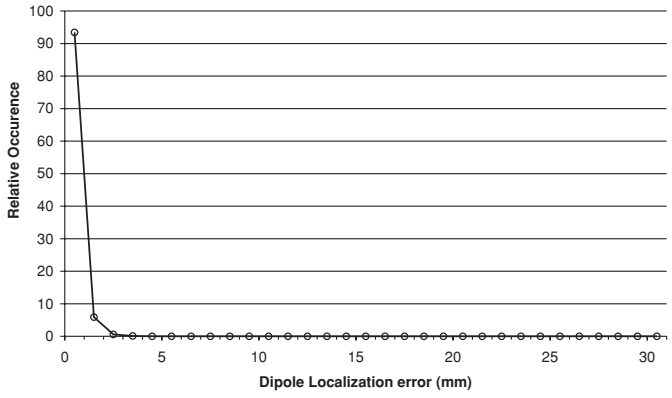

(c)

Figure 8. The histogram of the dipole localization error in the isotropic five-shell spherical head model using FDM-R at a grid size of (a) 3 mm, (b) 2 mm and (c) 1 mm. The dipole localization error is pointed out on the *X*-axis in mm. The *Y*-axis indicates the percentage of dipoles which belongs to a range of dipole localization errors indicated by the bin.

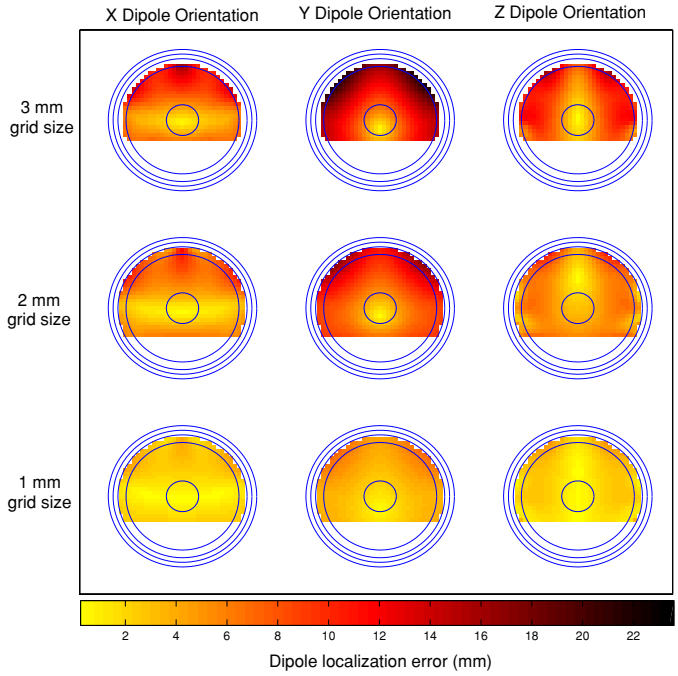

Figure 9. The dipole localization error for an anisotropic conducting skull layer is shown. The colour bar shows the distance from the original dipole to the estimated dipole in mm. The rows show the dipole localization error at a same grid size, while the columns show the dipole localization error when the original dipole orientation is considered fixed.

4. Results

4.1. Dipole localization errors due to omitting an anisotropic conductivity

Figure 5(a) shows the dipole localization error due to using an isotropic skull conductivity instead of an anisotropic one. The results are only shown for the *XY* plane of dipoles and a dipole orientation in the *X* direction. For the other cases we obtain similar results. The localization error is represented as an arrow in each test dipole position: the tail of the arrow shows the original position while the tip shows the fitted position. The arrow is projected on the plane, containing the test dipoles, as the error in the direction perpendicular to the plane is very small ($\leqslant$0.5 mm). The arrows at the grey matter outer sphere are pointing inwards indicating that the dipoles in that compartment are estimated towards the centre. Note that in the figure some of the arrows are not depicted to obtain a clearer presentation. Figure 5(b) shows the dipole localization error due to using an isotropic white matter conductivity instead of an anisotropic one in the same way as explained above. The dipoles in the inner grey matter compartment are estimated away from the centre, as is shown by the arrows. It is not clearly shown in figure 5, but due to the specific electrode configuration the overall results are not spherically symmetric. Figure 6 shows a histogram (bin width 2 mm) of the dipole localization error for not including skull and white matter anisotropy.

Omitting skull anisotropy gives rise to a mean localization error of 13.73 mm. Note that there are no errors larger than 25 mm. The histogram peaks around 17 mm.

In the case of omitting white matter anisotropy the mean localization error is 11.21 mm. Here, a more uniform distribution is observed.

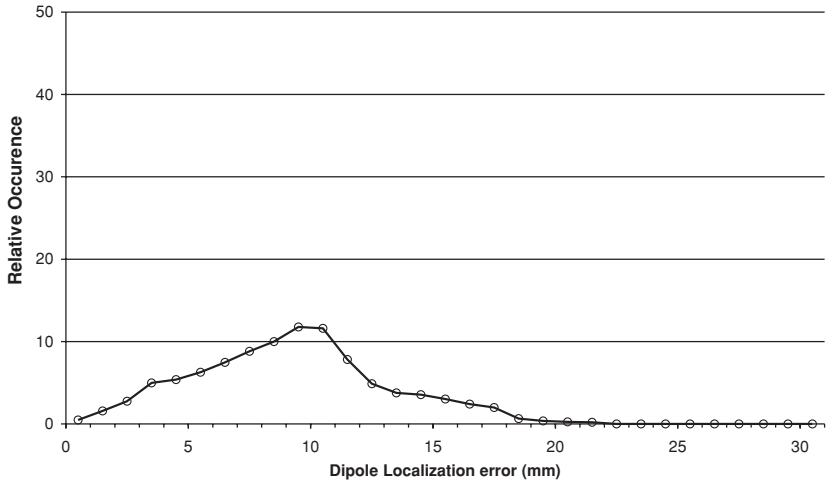

(a)

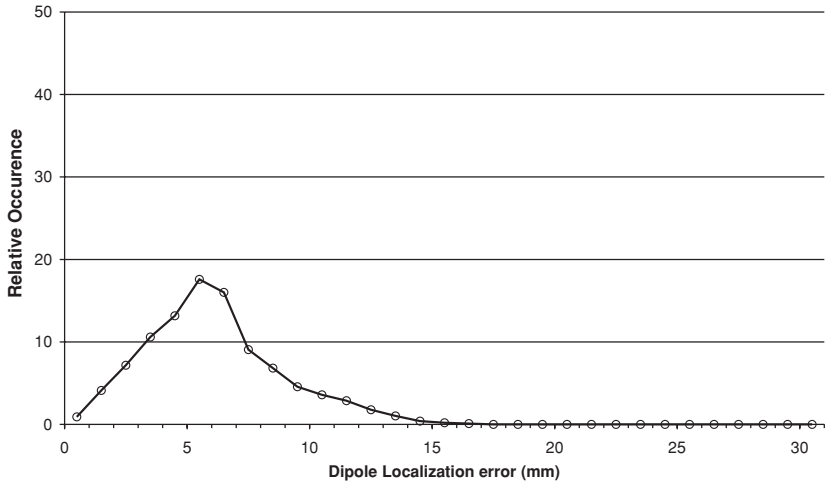

(b)

Figure 10. The histogram of the dipole localization errors for using FDM-R in a five-shell spherical head model with a skull anisotropic conducting compartment is shown at a grid size of (a) 3 mm, (b) 2 mm and (c) 1 mm, respectively. The dipole localization error is denoted on the *X*-axis in mm. The *Y*-axis indicates the percentage of dipoles which belongs to a range of dipole localization errors indicated by the bin. To place these results in a broader context, we also repeated (d) the histogram of the dipole localization errors due to using an isotropic instead of an anisotropic skull compartment.

4.2. Dipole localization errors due to using FDM-R in a five-shell spherical head model with isotropic conducting compartments

Each row in figure 7 represents the dipole localization error for a given grid size. We distinguish a 1, 2 and 3 mm grid. The three columns represent the errors for a fixed dipole orientation. The mean localization errors are 1.43 mm, 0.78 mm, 0.48 mm for a 3 mm, 2 mm and 1 mm grid size respectively. The colour indicates the dipole localization error. We can see that at

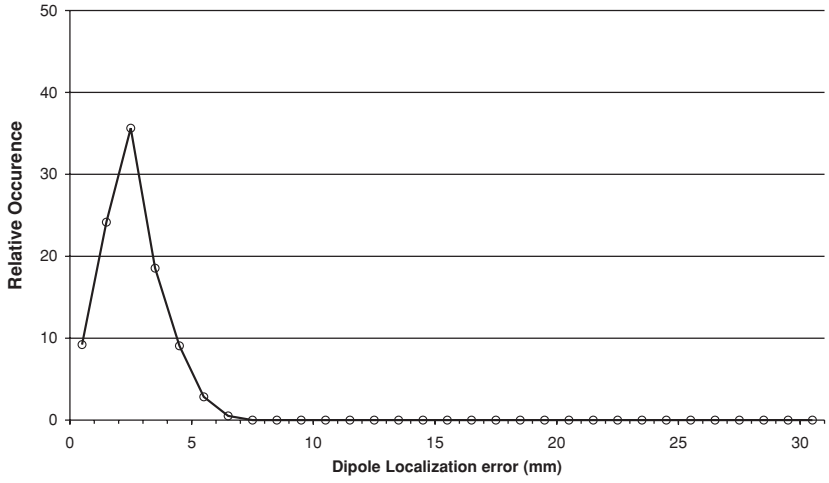

(c)

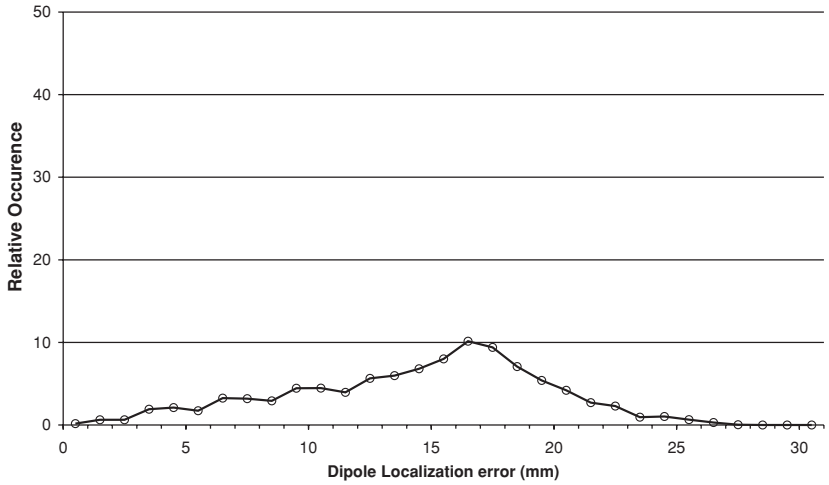

(d)

Figure 10. (Continued.)

a 3 mm grid size, the dipole localization errors are greater than a 2 mm grid size, which has greater dipole localization errors as a 1 mm grid size.

Figure 8 shows the histogram of the dipole localization error for (a) 1 mm grid size, (b) 2 mm grid size and (c) 3 mm grid size. The finer the grid, the more the distribution is skewed to the left. Note that for a 1 mm grid size there is no larger dipole localization error than 3 mm.

4.3. Dipole localization errors due to using FDM-R in a five-shell spherical head model with anisotropic conducting compartments

Figure 9 shows the dipole localization error when only skull anisotropy is incorporated in the FDM-R and spherical lead model, for dipole orientations along the Cartesian axes and

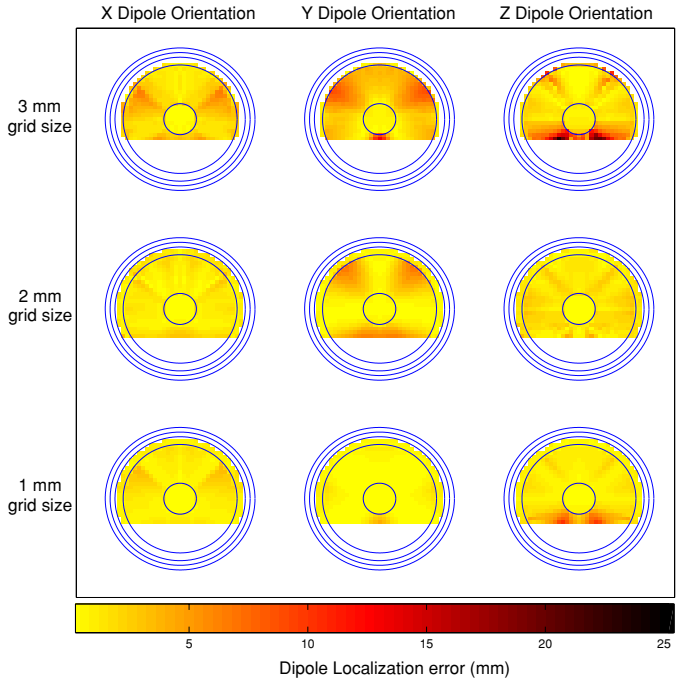

Figure 11. The dipole localization error if the white matter layer is anisotropic, is shown at different grid sizes. The colour denotes the distance between the original dipole and the estimated dipole in mm. The rows show the dipole localization error at a same grid size, while the columns show the dipole localization error when the original dipole orientation is considered fixed.

different grid sizes. We obtain a mean dipole localization error of 9.229 mm for a 3 mm grid size (standard deviation: 3.905 mm, maximum: 21.765 mm), 6.086 mm for a 2 mm grid size (standard deviation: 2.765 mm, maximum: 16.541 mm) and 2.551 mm for a 1 mm grid size (standard deviation: 1.192 mm, maximum: 6.793 mm). For a 3 mm grid size we see large dipole localization errors, which are located near the interface of the white matter shell and the grey matter outer shell. As the grid size decreases, the dipole localization errors decrease.

The histogram of the dipole localization error is given in figure 10. We can appreciate that the distribution of the errors shifts to the left, when moving from a coarse to a fine grid. It is important to note is that at a 1 mm grid size the dipole localization error has an upper boundary equal to 7 mm. To place these results in a broader context, we also repeated the histogram of the dipole localization error due to using an isotropic instead of an anisotropic compartment (see figure 10 (d)).

Figure 11 shows the dipole localization error when only white matter anisotropy is incorporated in the FDM-R and spherical head model, for dipole orientations along the three Cartesian axes and different grid sizes. We obtain a mean dipole localization error of 3.078 mm for a 3 mm grid size (standard deviation: 3.171 mm, maximum: 34.142 mm), 1.695 mm for a 2 mm grid size (standard deviation: 1.434 mm, maximum: 12.047 mm) and 1.044 mm for a 1 mm grid size (standard deviation: 1.107 mm, maximum: 11.606 mm). The dipole localization errors are smaller than those when only skull anisotropy is incorporated in the FDM-R. At a 3 mm grid size the dipole localization is worst at the basal part of the brain, below the centre. The histogram of the dipole localization error is shown in figure 12. We can

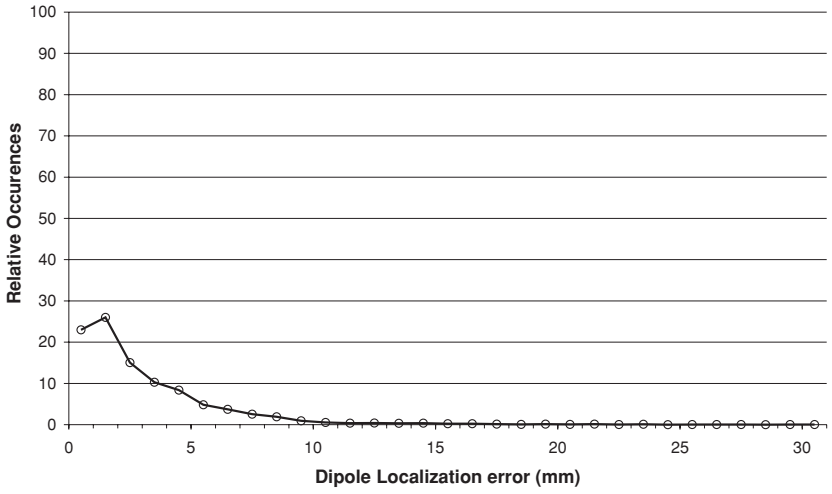

(a)

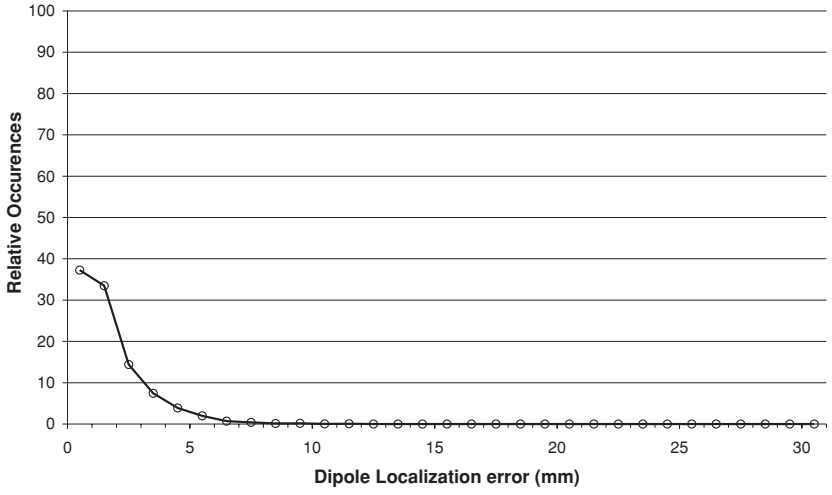

(b)

Figure 12. The histogram of the dipole localization errors for using FDM-R in a five-shell spherical head model with a white matter anisotropic conducting compartment is shown at a grid size of (a) 3 mm, (b) 2 mm and (c) 1 mm, respectively. The dipole localization error is denoted on the *X*-axis in mm. The *Y*-axis indicates the percentage of dipoles which belongs to a range of dipole localization errors indicated by the bin. To place these results in a broader context, we also (d) repeated the histogram of the dipole localization errors due to using an isotropic instead of an anisotropic white matter compartment.

see that the anisotropy is modelled very adequately. Moreover, the upper boundary of the dipole localization error at a 1 mm grid size is 6 mm.

5. Discussion

Firstly, we investigated the dipole localization errors due to using isotropic conducting compartments instead of an anisotropic one. We found that the dipole localization error

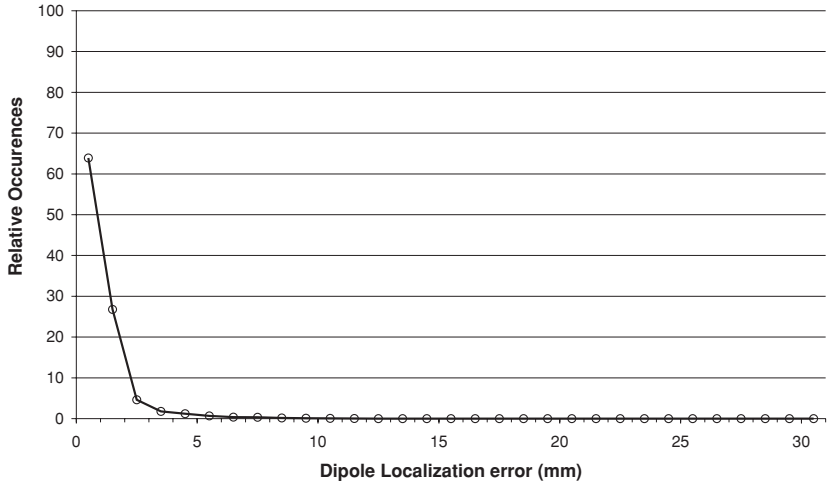

(c)

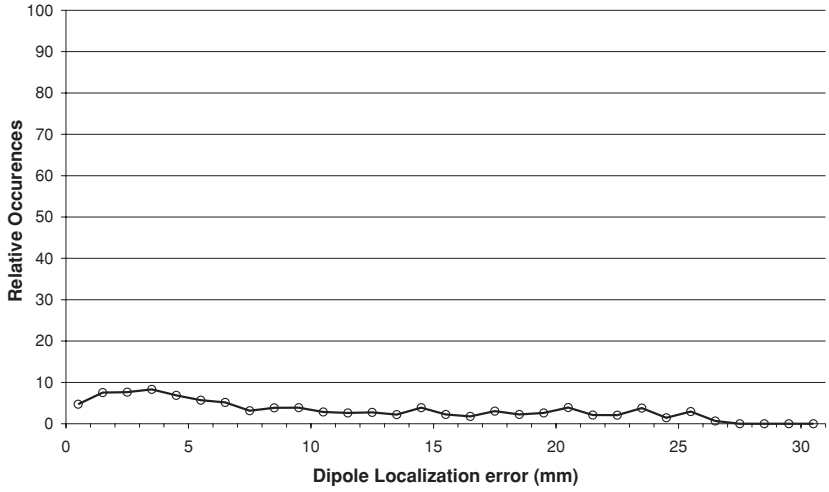

(d)

Figure 12. (Contined.)

is on average 13 mm and 11 mm for skull and white matter compartments respectively. Similar results were found by Haueisen *et al* (2002).

Secondly, we validated FDM-R for isotropic spherical head models. Other studies obtain mean localization errors of 3.4 mm and 2.2 mm, for a 3 and 2 mm grid size in a spherical head model (Vanrumste *et al* (2001). In the latter, FDM-R was also used, but the computational points were located at the centre of the elements. By moving the computational points to the nodes of the elements as shown here, we can obtain a smaller mean localization error of 1.43 mm, 0.78 mm and 0.48 mm for a 3 mm, 2 mm and 1 mm grid size respectively. We also used 18 neighbours instead of 6 to calculate the potentials which also could be more beneficial.

We also performed a validation study of the FDM-R in anisotropic spherical head models. To our knowledge no other study addressed this. Studies by Wolters (2003) and Zhang *et al*

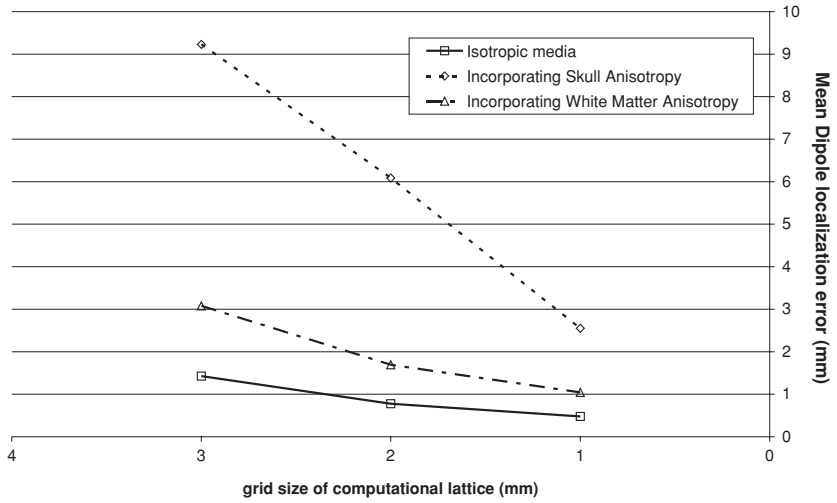

Figure 13. The mean dipole localization error due to discretization in head models with isotropic conducting compartments, with an anisotropic conducting skull compartment and with an anisotropic conducting white matter compartment as a function of the grid size.

(2004) mainly assess the effect on the forward problem by means of correlation coefficients, but do not perform an estimation of the dipole parameters.

Note as shown in figure 13 the dipole localization error when assuming anisotropic compartments is bigger than the dipole localization error when assuming isotropic compartments. In the anisotropic head models, there is not only a discretization of the potential values, like in the isotropic head models, but there is also a discretization of the conductivity tensors. In a numerical head model, an element belonging to an anisotropic compartment has a fixed matrix representation of the conductivity tensors. The conductivity tensors are dependent on the direction of the anisotropy, which is dependent on the vectors tangential to the skull surface for the skull anisotropy. These vectors are only calculated on discrete places in the skull layer. In reality, the vectors can be written as continuous functions.

The time needed to calculate the lead-field matrix using FDM-R in the present study was on average 10 min, 40 min and 14 h for a 3 mm, 2 mm and 1 mm grid size respectively. For a 1 mm grid size a lot of disc I/O was required to solve the forward problem due to memory limitations. Using the reciprocity theorem, the inverse problem is solved very fast. The time needed to estimate a dipole was on average 2–4 s. Algebraic multigrid (AMG) solvers can be used to improve the calculation time (Mohr and Vanrumste 2003).

We are aware that the white matter compartment is not realistically modelled. In this study, we assumed that the white matter fibres started at the edge of the inner grey matter sphere and spread radially to the edge of the outer grey matter sphere. In reality, the white matter fibres can also have a tangential direction, as is the case in the corpus callosum and in the formatio reticularis. One way to determine a more precise direction of white matter fibres is by fibre tracking in diffusion tensor images (DTI) (Tuch *et al* 2001, Tuch 2002).

Although the average dipole localization error for using, FDM-R with an anisotropic skull compartment is 2.5 mm, we still can note errors larger than 6 mm. Note, however, that the average localization error due to using isotropic instead of anisotropic compartments is 13.3 mm, which is about twice the worst case scenario of the performance of FDM-R.

The results shown in the present study indicate that FDM-R can be used for realistic head models. One way to do this is by dividing the head in cubes of a specific grid size. The smaller the grid size, the smaller the dipole localization error due to using FDM-R, but the larger the memory and computational needs. Once the head model is made the inverse problem can be solved. With the use of reciprocity, the number of forward calculations, needed to solve the inverse problem, can be reduced very significantly.

In the future we plan to use this numerical method in realistic head models with realistic anisotropic conductivity. This conductivity can be measured by a recently developed imaging modality: diffusion tensor magnetic resonance imaging. By using this technique, we can measure the direction of the anisotropy. We can subsequently calculate the anisotropic conductivities in the elements by means of the volume constraint. Here, we hope that the use of more realistic models results in a more accurate dipole estimation.

6. Conclusions

We investigated the influence of the anisotropic conductivities of brain tissues on EEG dipole analysis. Neglecting the skull anisotropy and white matter anisotropy yields mean dipole localization error of 13.73 mm and 11.21 mm, respectively. These errors are not negligible and the anisotropic conductivities have to be incorporated in the volume conductor model.

A validation of the FDM has been carried out in isotropic media. This was done by posing the conductivity tensors in each element as diagonal matrices. We investigated the performance of FDM-R by means of the dipole localization error. We varied the grid spacing of the lattice of the numerical method from 3 to 1 mm. We found that the mean dipole localization errors are very small: 1.48 mm, 0.78 mm and 0.48 mm for a grid size of 3 mm, 2 mm and 1 mm, respectively. As a rule of thumb we can conclude that the error is on average half the grid size. From this part of the study we can conclude that the method works for isotropical head models.

To our knowledge, we were the first to apply reciprocity to solve the forward problem in a volume conductor model with anisotropic compartments. The skull was modelled as an anisotropic layer, where the conductivity in the tangential direction was 10 times bigger than in the radial direction to the skull surface. In this case, we also compared the analytical head model with the numerical head model, both with the anisotropic skull layer by means of the dipole localization error. The results for the mean dipole localization error in a function of the grid size can be found in figure 13. For a grid size bigger than 1 mm, the mean dipole localization is bigger than 3 mm. This means that the above FDM method cannot adequately model the skull anisotropy if the grid size is bigger than 1 mm. In order to model the anisotropy adequately, we must consider the grid size of the lattice of the FDM to be 1 mm or less.

Acknowledgments

We would like to cordially thank Dr J C de Munck for providing an implementation for the analytical formula in spherical head models. We also thank the members of MEDISIP for the support. Our gratitude also goes to Professor Dr P Boon (MD, PhD) and the members of the ‘Experimental Neurophysiology group’ for their dedication. Hans Hallez is funded by a PhD grant from the Institute for the Promotion of Innovation through Science and Technology in Flanders (IWT-Vlaanderen). Bart Vanrumste is a postdoctoral fellow funded by the ‘Programmatorische Federale Overheidsdienst Wetenschapsbeleid’ of the Belgian Government.

Appendix

The anisotropic conductivity can be represented as ellipsoids. The radii of the ellipsoid denote the conductivity at each direction. For example, in the scalp we model the conductivity as isotropic: the conductivity in each direction is the same ($\rho_{\text{scalp}} = 0.33$ S m^{-1}) and this can be represented by a perfect sphere. If there is one direction in which the conductivity is higher than the other two, then a cigar-shaped ellipsoid occurs. With two principal directions the ellipsoid has an oblique shape.

The *volume constraint* (Wolters *et al* 2001) states that the volume of the isotropic conducting sphere must be equal to that of the anisotropic conducting ellipsoids:

$$\tfrac{4}{3}\pi\sigma_{\text{isotropic}}^3 = \tfrac{4}{3}\pi\sigma_1\sigma_2\sigma_3. \tag{A.1}$$

Skull. For the skull we model the conductivity as an oblique ellipsoid, which means that two of the principal directions are the same. These directions correspond to the tangential direction on the surface. Together with the fact that the tangential conductivity is modelled 10 times bigger than the radial conductivity we obtain the following system of equations,

$$\tfrac{4}{3}\pi\sigma_{\text{isotropic}}^3 = \tfrac{4}{3}\pi\sigma_t^2\sigma_r \tag{A.2}$$

$$10\sigma_{\text{rad}} = \sigma_{\text{tang}} \tag{A.3}$$

where $\sigma_{\text{isotropic}}$ is 0.020 S m^{-1} for the skull compartment. Using these equations, we can solve σ_t and σ_r yielding the conductivity in the tangential and radial direction respectively. Solving the equations yields a radial conductivity of $\sigma_r^{\text{skull}} = 0.004\,309$ S m^{-1} and a tangential conductivity of $\sigma_t^{\text{skull}} = 10\sigma_r^{\text{skull}} = 0.043\,09$ S m^{-1}

White matter. For white matter anisotropy we modelled that they spread in the radial direction. We obtain the following equations,

$$\tfrac{4}{3}\pi\sigma_{\text{isotropic}}^3 = \tfrac{4}{3}\pi\sigma_t^2\sigma_r \tag{A.4}$$

$$9\sigma_{\text{trans}} = \sigma_{\text{long}} \tag{A.5}$$

where $\sigma_{\text{isotropic}}$ is 0.33 S m^{-1} for the brain compartment. Solving these equations yield σ_t and σ_r or the conductivity in the transversal direction (tangential direction) and in the longitudinal direction of the nerve fibre (radial direction), respectively. The results are a radial conductivity of $\sigma_r^{\text{white matter}} = 1.4278$ S m^{-1} and a tangential conductivity of $\sigma_t^{\text{white matter}} = 0.158\,64$ S m^{-1}.

References

Barrett R, Berry M, Chan T F, Demmel J, Donato J, Dongarra J, Eijkhout V, Pozo R, Romine C and der Vorst H V 1994 *Templates for the Solution of Linear Systems: Building Blocks for Iterative Methods* 2nd edn (Philadelphia, PA: SIAM)

Boon P, D'Havé M, Vonck K, Baulac M, Vandekerckhove T and De Reuck J 1996 Dipole modeling in epilepsy surgery candidates *Epilepsia* **38** 208–18

Darvas F, Pantazis D, Yildirim E K and Leahy R 2004 Mapping human brain functions with meg and eeg: methods and validation *Neuroimage* **23** 289–99

de Munck J and Peters M 1993 A fast method to compute the potential in the multiphere model *IEEE Trans. Biomed. Eng.* **40** 1166–74

Ferree T, Eriksen K and Tucker D 2000 Regional head tissue conductivity estimation for improved eeg analysis *IEEE Trans. Biomed. Eng.* **47** 1584–92

Gonçalves S, de Munck J C, Verbunt J P A, Bijma F, Heethaar R and Lopes da Silva F 2003 In vivo measurement of the brain and skull resistivities using an eit-basedmethod and realistic models for the head *IEEE Trans. Biomed. Eng.* **50** 754–67

Haueisen J, Tuch D, Ramon C, Schimpf P, Wedeen V, George J and Belliveau J 2002 The influence of brain tissue anisotropy on human EEG and MEG *Neuroimage* **15** 159–66

Hinchey F 1976 *Vectors and Tensors for Engineers and Scientists* (New York: Wiley)

Huiskamp G, Vroeijenstijn M, van Dijk R, Wieneke G and van Huffelen A 1999 The need for correct realistic geometry in the inverse EEG problem *IEEE Trans. Biomed. Eng.* **46** 1281–7

Mohr M and Vanrumste B 2003 Comparing iterative solvers for linear systems associated with the finite difference discretisation of the forward problem in electroencaphalographic source analysis *Med. Biol. Eng. Comput.* **41** 75–84

Malmivuo J and Plonsey R 1995 *Bioelectromagnetism: Principles and Applications of Bioelectric and Biomagnetic Fields* (New York: Oxford University Press)

Press W, Teukolsky S, Vetterling W and Flannery B 1995 *Numerical Recipes in C* (Cambridge: Cambridge University Press) pp 430–43

Rush S and Driscoll D 1969 EEG electrode sensitivity—an application of reciprocity *IEEE Trans. Biomed. Eng.* **16** 15–22

Saleheen H and Kwong T 1997 New finite difference formulations for general inhomogeneous anisotropic bioelectric problems *IEEE Trans. Biomed. Eng.* **44** 800–9

Saleheen H and Kwong T 1998 A new three-dimensional finite-difference bidomain formulation for inhomogeneous anisotropic cardiac tissues *IEEE Trans. Biomed. Eng.* **45** 15–24

Salu Y, Cohen L G, Rose D, Sato S, Kufta C and Hallett M 1990 An improved method for localizing electric brain dipoles *IEEE Trans. Biomed. Eng.* **37** 699–705

Sarvas J 1987 Basic mathematical and electromagnetic concepts of the biomagnetic inverse problem *Phys. Med. Biol.* **32** 11–22

Scherg M 1992 Functional imaging and localization of electromagnetic brain activity *Brain Topogr.* **5** 103–11

Tuch D 2002 Mapping cortical connectivity with diffusion MRI *IEEE Int. Symp. Biomedical Imaging: Macro to Nano (July)* pp 392–4

Tuch D, Wedeen V, Dale A, George J and Belliveau J 2001 Conductivity tensor mapping of the human brain using diffusion tensor MRI *Proc. National Academy of Science (Sept.)* vol 98, pp 11697–701

Vanrumste B, Van Hoey G, Van de Walle R, D'Have M, Lemahieu I and Boon P 2000 Dipole location errors in electroencephalogram source analysis due to volume conductor model errors *Med. Biol. Eng. Comput.* **38** 528–34

Vanrumste B, Van Hoey G, Van de Walle R, D'Havé M, Lemahieu I and Boon P 2001 The validation of the finite difference method and reciprocity for solving the inverse problem in eeg dipole source analysis *Brain Topogr.* **14** 83–92

Wolters C 2003 Influence of tissue conductivity inhomogeneity and anisotropy on EEG/MEG based source localization in the human brain *PhD Thesis* Universität Leipzig

Wolters C, Anwander A, Koch M, Reitzinger S, Kuhn M and Svensen M 2001 Influence of head tissue conductivity anisotropy on human EEG and MEG using fast high resolution finite element modeling, based on a parallel algebraic multigrid solver *Forschung und wissenschaftliches Rechnen, Contributions to the Heinz-Billing Award, Gesellschaft für wissenschaftliche Datenverarbeitung mbH Göttingen* pp 111–57

Yvert B, Bertrand O, Thëvenet M, Echallier J and Pernier J 1997 A systematic evaluation of the spherical model accuracy in eeg dipole localization *Electroencephalogr. Clin. Neurophysiol.* **120** 452–9

Zhang Y C, Zhu S A and He B 2004 A second-order finite element algorithm for solving the three-dimensional EEG forward problem *Phys. Med. Biol.* **49** 2975–87